Research Square

Preprints are preliminary reports that have not undergone peer review.
They should not be considered conclusive, used to inform clinical practice,
or referenced by the media as validated information.

Continuous glucose monitoring earbuds for periodic metabolic sensing

Joseph Wang

josephwang@ucsd.edu

University of California San Diego https://orcid.org/0000-0002-4921-9674

Barak Sabbagh

University of California, San Diego https://orcid.org/0009-0009-5682-5144

Christian Gosti

University of Rome Tor Vergata

Ellen V Stadler

Imperial College London

Madeleine McSwain

University of California San Diego

Lauren Chiu

University of California San Diego

Muhammad Inam Khan

University of California San Diego https://orcid.org/0009-0002-1216-8137

Qinyu Yu

University of California San Diego

Victor Perez

University of California San Diego

Tamoghna Saha

University of California, San Diego https://orcid.org/0000-0002-0753-3577

Gaoyuan Ji

University of California San Diego https://orcid.org/0009-0006-1343-6921

Minjoon Park

University of California San Diego https://orcid.org/0009-0005-9772-6346

Kavya Garg

University of California San Diego

Parth Bhagwat

University of California San Diego

Yi Fung Winsten Lam

University of California San Diego https://orcid.org/0009-0008-4823-1138

Omeed Djassemi

University of California San Diego https://orcid.org/0009-0004-6061-3316

Maria Reynoso

University of California San Diego

Fabiana Arduini

University of Rome Tor Vergata

Article

Keywords:

Posted Date: November 11th, 2026

DOI: https://doi.org/10.21203/rs.3.rs-11505206/v1

License: This work is licensed under a Creative Commons Attribution 4.0 International License.
Read Full License

Additional Declarations: There is **NO** Competing Interest.

Continuous glucose monitoring earbuds for periodic metabolic sensing

Barak Sabbagh[a‡], Christian Gosti[a,b‡], Ellen V Stadler[a,c‡], Madeleine McSwain[d], Lauren Chiu[a], Muhammad Inam Khan[a], Qinyu Yu[a], Victor Perez[e], Tamoghna Saha[a], Gavin Ji[a], Minjoon Park[a], Kavya Garg[a], Parth Bhagwat[e], Yi Lam[a], Omeed Djassemi[a], Maria Reynoso[a], Fabiana Arduini[b], and Joseph Wang[a*]

[a] Aiiso Yufeng Li Family Department of Chemical and Nano Engineering, University of California San Diego, La Jolla, CA 92093, USA

[b] Department of Chemical Sciences and Technologies, University of Rome "Tor Vergata" Via della Ricerca Scientifica, 00133 Rome, Italy

[c] Department of Infectious Diseases, Imperial College London, London, UK.

[d] Department of Electrical Engineering, University of California San Diego, La Jolla, California 92093, USA

[e] Department of Mechanical Engineering, University of California San Diego, La Jolla, California 92093, USA

[‡] Equal contribution

[*] Corresponding Author, J.W. E-mail: josephwang@ucsd.edu

Abstract

The applications of continuous glucose monitoring (CGM) are expanding into wellness, sports and preventive health, where metabolic information is particularly valuable around specific physiological events. However, conventional CGMs remain tailored to diabetes management, requiring around-the-clock, fixed wear even when periodic monitoring is sufficient. Here, we introduce the continuous glucose in-ear monitor (cGEM), an earbud-integrated platform for periodic, on-demand glucose monitoring from in-ear sweat. The cGEM establishes a skin–sensor interface through simple insertion and removal, enabling repeated monitoring without adhesive fixation. The platform integrates osmotic sweat extraction, microfluidic sampling and electrochemical glucose sensing while retaining audio playback. Computational modelling and in vitro characterization demonstrated controlled fluid transport and reliable glucose sensing. Dual-channel adaptive noise cancellation and personalized calibration reduce on-body signal artifacts and account for individual differences in blood–sweat glucose relationships. Despite periodic use, the cGEM showed close agreement with a continuously worn commercial CGM, achieving a mean absolute relative difference (MARD) of 8.79% across more than 50 h of monitoring. Repeated 1.5–5 h sessions captured event-specific glucose responses with a Pearson correlation coefficient of r = 0.88 relative to the commercial CGM. By integrating molecular sensing into widely used wireless earbuds, cGEM opens new possibilities for widespread adoption of metabolic monitoring, making it as accessible and routine as listening to music.

Introduction

Wearable health technologies are rapidly evolving from tracking activity and vital signs to continuous molecular monitoring[1]. Among these, continuous glucose monitors (CGMs) have transformed diabetes management by enabling real-time glucose tracking, reducing reliance on finger-prick testing, and supporting personalized care[2–5]. Building on this success, growing interest in glucose dynamics for wellness, sport, preventive health, and metabolic assessment is expanding the potential role of CGMs beyond people with diabetes to the general population[6,7]. Yet, despite their commercial availability and established clinical performance, broader routine use of CGMs among the general population remains limited[8]. This limitation reflects the physical burden of minimally invasive sensors and adhesive patches, the psychological burden associated with prolonged device wear, and the cost of dedicated monitoring devices, together contributing to reduced user comfort and accessibility[9–11]. While around-the-clock continuous glucose monitoring using prolonged fixed-wear devices is critical for type 1 diabetes management[12–14], many of the emerging applications (e.g., wellness, sport) may instead benefit from periodic, user-initiated monitoring during select physiologically informative periods[12]. This gap motivates the development of glucose monitoring technologies that bridge single-point finger-prick measurements and prolonged CGM wear. Such platforms could enable continuous glucose assessment during extended preselected user-defined periods without requiring persistent device attachment. They should be unobtrusive, user-friendly, easily placed and removed, while delivering accurate sensing across repeated sessions[15–17].

Sweat provides a promising non-invasive biofluid for monitoring metabolites such as glucose[17–20]. Sweat glucose has been shown to reflect blood and interstitial-fluid glucose dynamics, although at lower absolute concentrations and with a temporal lag[21–23]. A broad range of epidermal wearable platforms, including tattoo-based sensors[24,25], flexible microfluidic systems[21,26,27], paper-based devices[23,28–30], textile patches[31,32], and electrode-hydrogel interfaces[33–35], have demonstrated the feasibility of continuous sweat-based glucose monitoring[23,30]. These advances increasingly combine flexible electronics, advanced materials, microfluidics, wireless communication, and real-time analysis[36–39]. Despite this progress, most approaches still rely on dedicated skin-mounted platforms that require fixed body attachment and are often positioned at less convenient locations for the user. These factors increase user burden and limit routine adoption and compliance in everyday life. Beyond usability, fixed skin-mounted sensing is further challenged by variable adhesion, motion-induced interface changes, and fluctuations in sweat availability[40].

Embedding biosensing capabilities into widely adopted entertainment wearables offers one route toward a broader and more socially acceptable approach for molecular monitoring[41]. True wireless stereo (TWS) earbuds are particularly compelling as they are already widely

adopted in daily life and designed for comfort and repeated wear[42]. Their routine placement and removal make them naturally suited to periodic, user-defined sensing. Their widespread adoption also facilitates the integration of biosensors into everyday consumer devices. Accordingly, ear-worn devices have already emerged for vital sign monitoring, including cardiovascular and respiratory monitoring[43,44], core-body temperature tracking[45], and neurological assessment[42,46–48]. Yet, their potential for molecular health monitoring remains comparatively underexplored[45].

Here we report a continuous glucose in-ear monitor (cGEM), an earbud-integrated platform for periodic, non-invasive glucose monitoring from in-ear sweat during user-defined sensing periods (Fig. 1a,b). Unlike conventional CGMs and skin-mounted glucose sensors[52-54], cGEM establishes a glucose-sensing interface through simple earbud insertion and removal, enabling user-defined monitoring without adhesive fixation while retaining earbuds' native ergonomic design and entertainment function. Its disposable sensing module combines an enzymatic electrochemical (eChem) glucose biosensor with a hydrogel–paper fluidic system (Fig. 1c). To address limited in-ear sweat availability and controlled analyte transport, we engineered a multimodal sampling strategy, integrating osmotic extraction, capillary transport, and evaporation-driven flow to continuously deliver fresh sweat to the sensing interface (Fig. 1d). Finite-element modeling, in vitro characterization, and on-body experiments were used to assess fluid and analyte transport, showing consistent transport behavior across conditions representative of routine earbud use.

To improve sensing reliability at the ear–sensor interface, cGEM incorporates an enzyme-free reference sensor for adaptive noise cancellation of common-mode artifacts arising from changes in pressure, position, and motion (Fig. 1e). The cGEM achieves high integration within the original compact earbud form factor. The glucose biosensor and fluidic system are combined with miniaturized electronics, including a low-power potentiostat, microcontroller, Bluetooth communication module, and rechargeable battery, while retaining the audio components required for standard audio playback (Fig. 1f). Personalized calibration further accounts for individual sweat-to-blood glucose relationships and physiological time delays. In human studies, the cGEM demonstrated close agreement with a commercial CGM and supported glucose tracking during user-defined monitoring sessions spanning short- to extended-duration periods (Fig. 1g,h). Despite being worn only periodically rather than continuously throughout the day, the cGEM captured glucose responses to specific events, such as meals, beverages, and physical activity, with 98% of paired measurements falling within Zone A of the Clarke error grid relative to the commercial CGM. Together, these findings establish a new paradigm for periodic glucose monitoring, turning everyday earbuds into a powerful metabolic sensing platform that combines

biochemical monitoring with entertainment, paving the way for accessible metabolic monitoring among the general population.

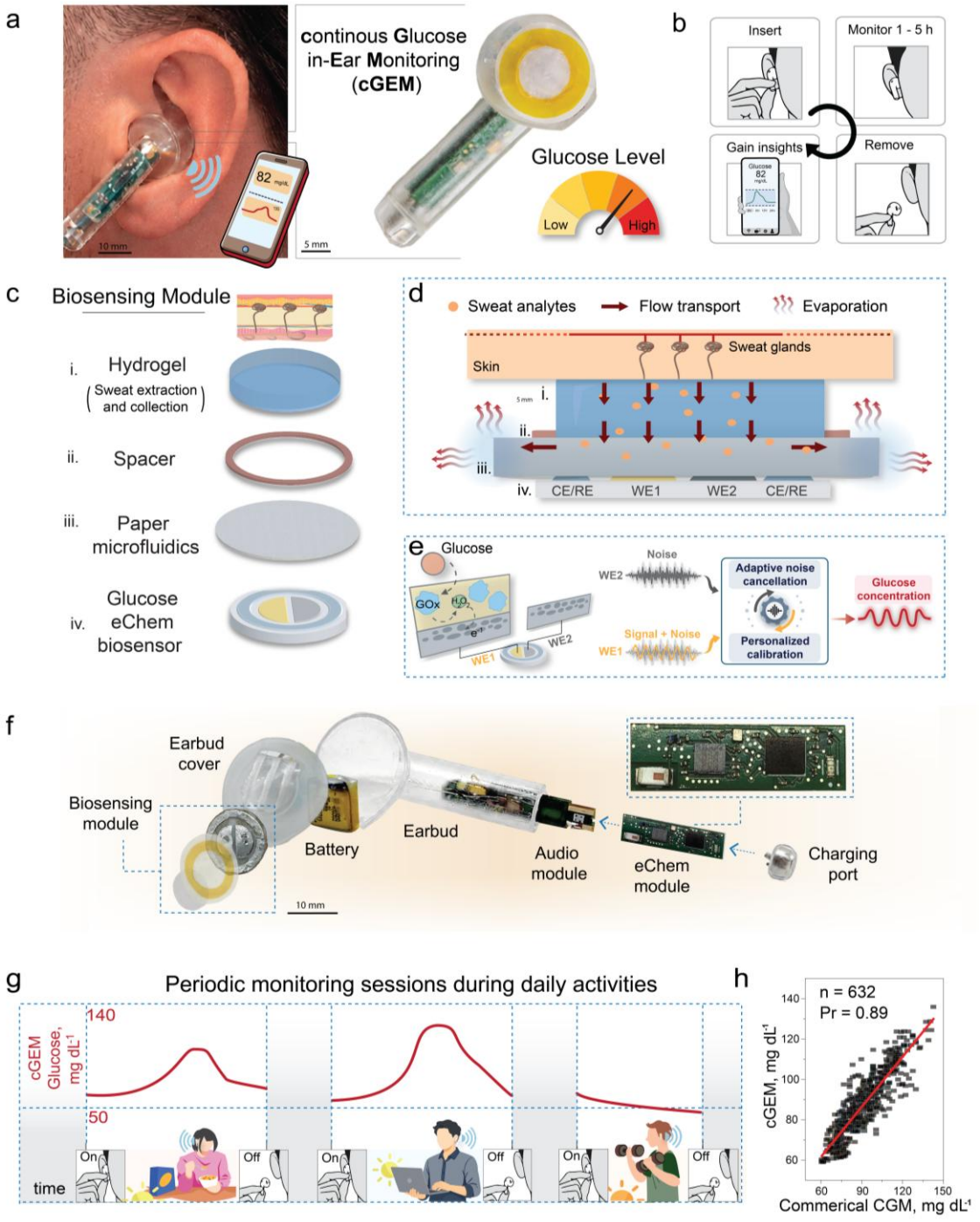


Figure 1: An earbud-integrated platform for sweat-based continuous glucose in-ear monitoring (cGEM). ***a)*** *Photos of the cGEM earbuds and their use.* ***b)*** *Periodic cGEM use throughout the day, with plug-and-play operation whenever desired: insert, monitor, remove*

and gain insight. ***c)*** *Exploded-view schematic of the biosensing module, showing (from bottom to top) the dual channel glucose biosensor, radial paper-based microfluidics, spacer layer, and hydrogel interfacing the ear skin.* ***d)*** *Cross-sectional illustration of the biosensing assembly, showing the continuous osmotic and evaporation-driven flow (red arrows) and the corresponding transport of sweat and its analytes (orange dots) from the skin, through the hydrogel (i), with the spacer (ii) defining the exposed evaporation area, and through the paper microfluidic channel (iii) toward the sensor (iv) and paper edge.* ***e)*** *Schematic of the dual-channel glucose biosensor. WE1 is functionalized with GOx and measures the glucose-dependent signal together with shared noise, whereas enzyme-free WE2 serves as a reference channel for noise alone. The two signals are processed by adaptive noise cancellation, and the corrected output is converted to glucose concentration using personalized calibration.* ***f)*** *Exploded-view photograph of the cGEM earbud, showing the earbud housing, biosensing module, eChem PCB module, battery, audio module, and charging port.* ***g)*** *Representative periodic cGEM monitoring sessions performed throughout the day across different daily activities.* ***h)*** *Comparison of cGEM with a commercial CGM. Whereas the commercial CGM remained continuously attached to the body for ~one week, the cGEM was worn only during each sensing session and removed immediately afterward. The two systems showed a Pearson correlation coefficient of r = 0.89 across >650 paired measurements acquired at 5-min intervals, with sensing sessions ranging from 1.5 to 5 h.*

Results

Design and Operation of the fluidic patch for cGEM

The fluidic patch was designed for real-time, continuous glucose monitoring at ultra-low sweat secretion rates (~nL min^{-1}) within a compact, earbud-compatible form factor. The assembled fluidic patch, including its cross-sectional architecture and corresponding numerical model of coupled fluid and mass transport, is shown in Figure 2a. The fluidic patch comprises a circular cellulose paper layer (2 cm diameter) interfaced centrally with an agarose hydrogel on the skin-facing side and sensing electrodes on the opposite side (Figure 2a). Upon hydrogel-paper contact, capillary wicking rapidly hydrates the full paper (~50 s, Fig. S1), after which evaporation drives continuous radial flow across the sensing region (Figure 2b-i). To sustain this flow and paper hydration over time, the hydrogel contains excess fluid and acts as a reservoir (Fig. S1). At the skin-facing interface, the hydrogel directly contacts the ear skin, enabling localized sweat collection (Figure 2b-ii). Sweat availability at this interface is supported by natural perspiration[47] and osmotic extraction[23,49]. Natural perspiration has previously been demonstrated to provide sufficient sweat for biosensing within the ear[47], while incorporation of 20% ethylene glycol into the hydrogel promotes additional sweat extraction by establishing an osmotic gradient across the skin–hydrogel interface (Fig. S2). The induced radial flow advectively transports sweat analytes across the sensing electrodes (Fig. 2b-iii) and subsequently carries them away, continuously

replenishing the sensing region with fresh fluid (Fig. 2b-iv). Inspired by prior demonstrations of evaporation-driven transport in epidermal sensing[50,51], a thin ring-shaped isolation layer was used to regulate flow by defining the exposed evaporation area of the paper (Fig. 2c). Sweat transport was experimentally mimicked by placing a 1 µL blue-dye droplet on the skin-facing side of the hydrogel and tracking its propagation through the paper under different isolation-layer configurations (Fig. 2c). Corresponding numerical simulations were subsequently performed under equivalent conditions (Fig. 2c). Increasing the exposed evaporation area from ~0 to 2.4 cm^2 (maximum evaporation; no isolation layer) increased the flow rate from ~135 nL min^{-1} to ~490 nL min^{-1}, respectively (Fig. 2d). This strong dependence on exposed area confirms that transport was governed predominantly by evaporation. Each of the examined configurations maintained a nearly constant flow rate over the first 90 min, with larger paper–hydrogel contact areas and hydrogel sizes further increasing the flow rate (Fig. S3). Long-term measurements revealed a trade-off between evaporation-induced transport rate and the duration of stable operation (Fig. 2e). A decline in paper hydration indicated that hydrogel replenishment no longer compensated for evaporative loss, marking the onset of transport instability. Operation was considered sustainable while paper hydration, determined by weighing the paper relative to its fully saturated state, remained above 90%. Accordingly, higher evaporation rates shortened operation to 5 h due to faster paper dehydration, whereas lower rates extended operation with a high paper hydration for up to ~10 h (Fig. 2e). An intermediate evaporation area of 1.4 cm^2 was therefore selected to minimize transport lag while maintaining prolonged operation compatible with routine earbud use, providing ~275 nL min^{-1} flow for up to 9 h. Consistently, on-body testing of the fluidic patch showed stable flow at ~150 nL min^{-1} across device orientations and during both rest and moderate cycling, confirming that evaporation-driven flow was maintained during wear (Fig. 2f and Fig. S4).

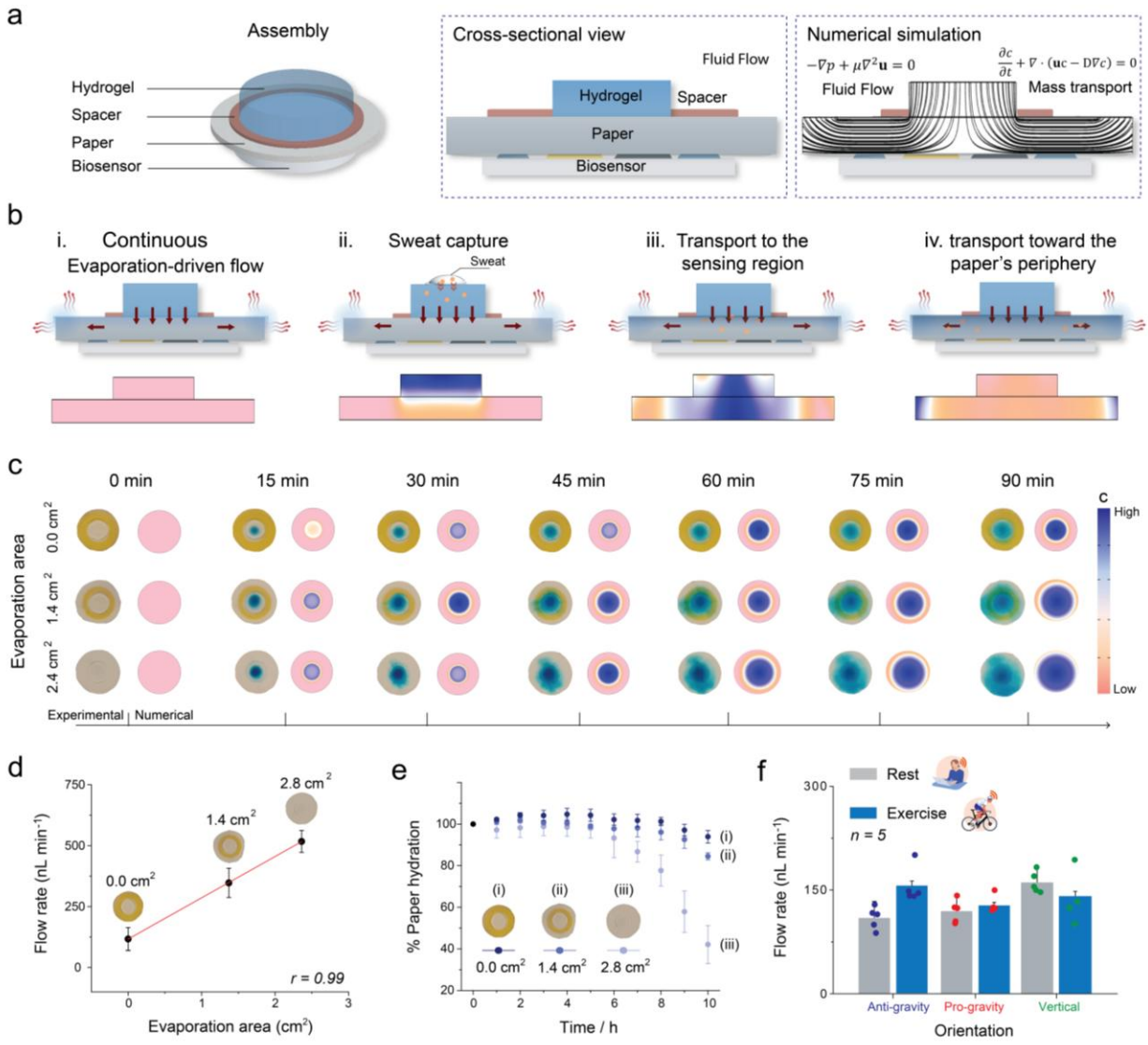


Figure 2: Design, transport mechanism, and in-vitro and-in vivo characterization of the cGEM fluidic patch. a) *Design, cross sectional view, and numerical model, including the governing Navier–Stokes and Nernst–Planck equations and calculated flow streamlines. All cross-sectional views are not drawn to scale.* ***b)*** *Transport mechanism (dimensions not to scale). Schematic illustration of the fluid-transport process, including continuous evaporation-driven flow* ***(i)****, sweat collection by the hydrogel upon generation at the skin interface* ***(ii)****, advective transport of glucose-containing sweat across the sensing region* ***(iii)****, and subsequent transport toward the paper's periphery* ***(iv)****. Corresponding numerically calculated spatiotemporal analyte-concentration profiles are shown below each step.* ***c)*** *Evaporation-controlled fluid transport. Experimental and numerical visualization of radial transport in the paper for exposed evaporation areas ranging from ~0 to 2.4 cm². Experimentally, a 1 µL blue-dye solution was introduced at the skin-interfacing side of the hydrogel, and its radial propagation through the paper was imaged from the bottom at 15-min intervals starting at 0 min. Details of the calculation are provided in Table S1. Numerical*

simulations show the corresponding spatiotemporal analyte-concentration maps under the same conditions and viewing orientation. ***d)*** *Flow-rate characterization under the three evaporation conditions shown in c, demonstrating a linear increase in transport rate with increasing exposed evaporation area.* ***e)*** *Paper hydration over extended operation time under the three evaporation conditions. Paper hydration was quantified hourly as the percentage of paper mass relative to its initial fully saturated state.* ***f)*** *On-body evaluation of fluid transport using the optimized geometry during rest (light bars) and mild cycling (dark bars) across three device orientations relative to gravity: horizontal pro-gravity (−90°), vertical (0°), and horizontal anti-gravity (90°). Flow rates were quantified over 90 min by tracking blue-dye transport, as in c, with mean flow rates summarized, demonstrating nearly constant flow across all cases.*

Glucose sensor characteristics

A non-invasive eChem glucose biosensor was developed on a flexible styrene–ethylene–butylene–styrene (SEBS) substrate for conformal placement in the ear and integration with the earbud (Fig. S5 and Video S1). coin-shaped, PCB-inspired two-layer sensor architecture uses conductive vias to connect the sensing and interconnection layers, reducing the footprint and eliminating lateral connections (Fig. 3a and Fig. S5-6). The sensing interface comprises two semicircular Pt working electrodes (WE1 and WE2) with a shared annular Ag/AgCl reference/counter electrode (RE/CE) (Fig. 3a). WE1 serves as the glucose-sensing electrode, whereas WE2 functions as an enzyme-free reference channel for adaptive noise cancellation. WE1 thus carries the enzymatic glucose detection through selective oxidation by glucose oxidase (GOx)[52] immobilized via Glutaraldehyde (GA) crosslinking[53]. The generated hydrogen peroxide is subsequently detected amperometrically (Fig. 3b). Electrodeposited nanostructured Pt enhanced hydrogen peroxide electrocatalysis at the electrode surface (Fig. 3c and Fig. S7). Glucose detection was evaluated using the Pt–GOx–GA sensor (WE1) against the enzyme- and reagent-free Pt sensor (WE2) (Fig. 3d). For chronoamperometric (CA) sensing, a potential of +0.3 V versus Ag/AgCl was selected based on sensitivity, selectivity, and signal-to-noise performance (Fig. S8 and Table S2). Consistent with this operating potential, cyclic voltammetry (CV) measurements showed the onset of hydrogen peroxide oxidation at +0.3 V for WE1 upon glucose addition, whereas WE2 exhibited no distinct oxidation peak (Fig. 3d). Across a concentration range relevant to sweat glucose sensing (0.01–2 mM), WE1 exhibited concentration-dependent responses with a sensitivity of 0.975 μA mM^{-1}, R^2 = 0.97, and a 7 μM limit of detection (LOD), whereas WE2 remained largely unresponsive (Fig. 3d). This process was systematically repeated across a range of Pt electrodeposition cycles (Fig. S7), and the optimized condition yielding maximal sensitivity is presented herein. The WE1 electrode showed negligible responses to potential interferents in sweat compared to glucose (Fig. 3e, Table S2) and retained 97% of its response over 14 h of operation (RSD 2.5%, Fig. 3f) without appreciable drift, fouling, or

enzyme leaching. The sensor also maintained reproducible performance over one week of storage and across varying environmental conditions, including temperature and humidity (Fig. S9). Validation against a commercial glucometer showed close agreement with our glucose biosensor across the tested glucose range (Fig. 3g). When integrated with the fluidic module, continuous flow prevented analyte accumulation during repeated glucose additions and enabled reversible responses through solution replenishment (Fig. 3h), unlike static conditions, where the signal progressively increased with each addition (Fig. 3i). These results validate the role of the integrated fluidic system in maintaining accurate continuous glucose monitoring.

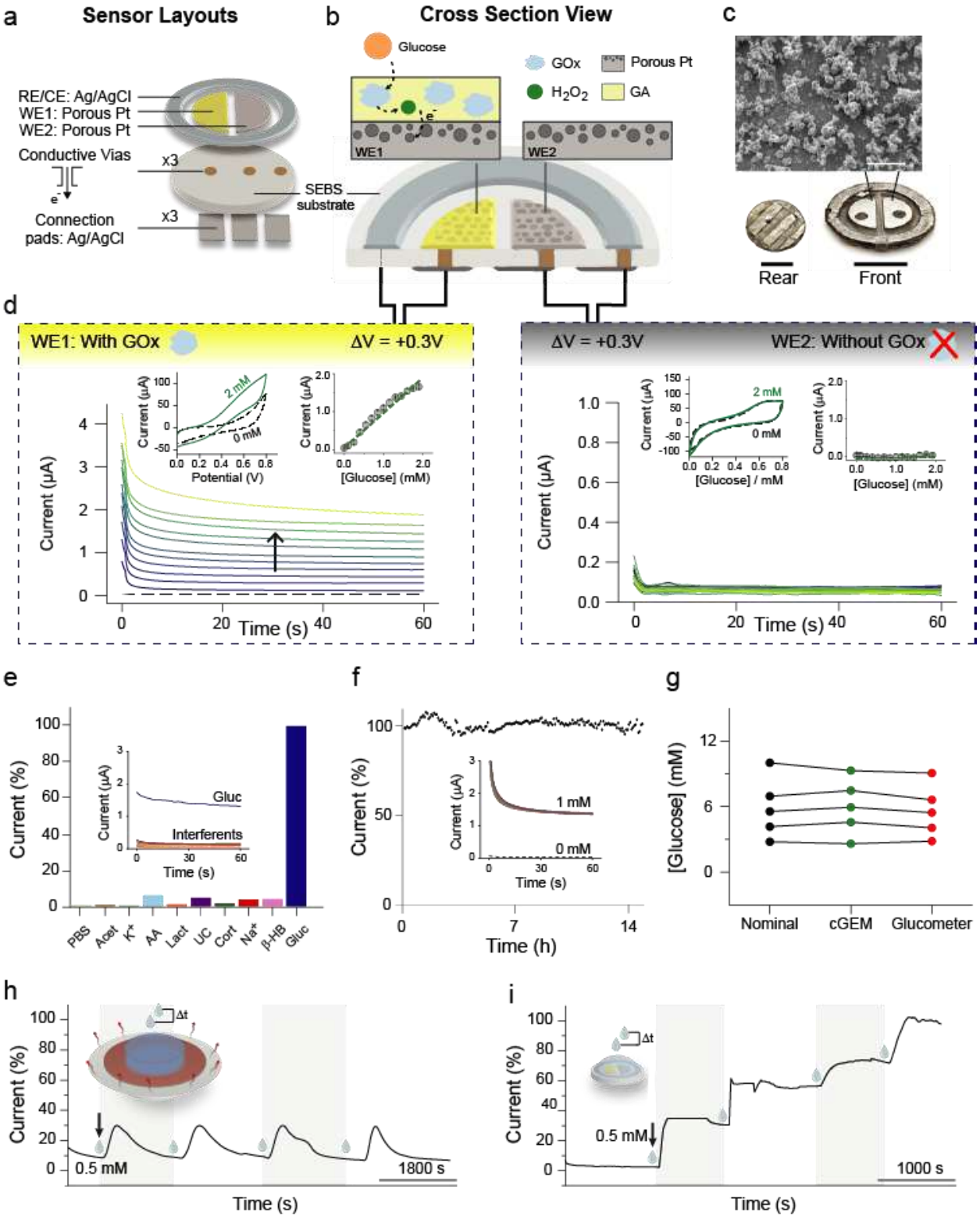


Figure 3: Design, sensing mechanism, and in vitro characterization of the cGEM biosensing platform. *a) Schematic of the layered sensor architecture, comprising two Pt working electrodes (WE1 and WE2) and a shared Ag/AgCl reference/counter electrode*

(REF/CE) patterned on the upper surface of a coin-shaped SEBS substrate. Three corresponding electrical contact pads are located on the SEBS underside, with conductive vias providing electrical connection between the bottom contact pads and the top electrodes. ***b)*** *Schematic illustration of the glucose-sensing mechanism at the enzyme-modified (WE1) and enzyme-free (WE2) working electrodes. WE2 served as a control channel (noise only) for adaptive noise cancellation.* ***c)*** *Representative photographs and scanning electron microscopy (SEM) images of the working-electrode surface after electrodeposition of Pt. Scale bar for sensor, 4.5 mm; SEM scale bar, 5 µm.* ***d)*** *Electrochemical response to glucose additions for the GOx-functionalized electrode (WE1, left) and the enzyme-free electrode (WE2, right). For each electrode, cyclic voltammograms (CVs) are shown before and after the addition of 2 mM glucose, together with chronoamperometric (CA) responses to successive 200 µM glucose additions from 0 to 2 mM, along with the corresponding calibration curve (inset). For GOx-functionalized WE1, the sensitivity was 0.975 µA mM* $^{-1}$ *with* R^2 *= 0.97, based on >40 measurements.* ***e)*** *Selectivity of the glucose biosensor (WE1), expressed as the relative current change following sequential additions of PBS, 500 µM acetaminophen (Acet), 2 mM potassium ions (*K^+*), 200 µM ascorbic acid (AA), 2 mM lactate (Lact), 200 µM uric acid (UA), 500 nM cortisol (Cort), 10 mM sodium ions (*Na^+*), 200 µM β-hydroxybutyrate (BHB), and 2 mM glucose (Gluc). The inset shows the corresponding raw CA response.* ***f)*** *Signal stability across 680 CA measurements acquired every 5 min in 1 mM glucose, showing <2% signal degradation over 14 h. The inset shows representative CA traces recorded hourly.* ***g)*** *Comparison of glucose concentrations calculated from the cGEM calibration curve to measurements from a commercial glucometer and the nominal glucose concentration.* ***h,i)*** *Continuous CA measurements acquired every 2 s following repeated 0.5 mM glucose additions performed without (h) and with (i) the developed fluidic patch.*

System Architecture and Integration

The fully integrated cGEM platform incorporates the disposable biosensing module, comprising of the glucose biosensor and fluidic patch, with reusable earbud electronics for real-time eChem signal acquisition (Fig. 4a,b and Figure S10-11). The platform was designed to accommodate variations in ear anatomy across users, similar to conventional commercial earbuds (Figure S12). The sensing board integrates a high-precision, low-power AD5940 analog front-end (AFE), an ultra-low-power nRF52832 system-on-chip (SoC), and 2.4-GHz RF front end (Figure S13-14 and Table S3). This configuration enables sequential acquisition from the two working electrodes and wireless transmission to a computer or cellphone (Fig. 4b). During CA measurements, the AFE applied a programmable +0.3 V bias, digitizing the resulting currents, while the SoC controls timing, processing, and communication. A 2.4-GHz monopole antenna supports wireless data transfer, with no measurable crosstalk between WE1 and WE2 or interference between sensing and audio electronics (Fig. S15). The system is powered by a 3.7 V, 60 mAh rechargeable Li-ion battery and consumes an average of 48 µW. It supports up to 5 h of continuous operation and can

be recharged through a customized charging interface (Fig. S15-S16 and Video S2). The potentiostat sensing terminals are permanently connected to conductive pads printed on a SEBS layer mounted to the earbud head, which serves as the interface for the disposable sensing module (Fig. S11). The disposable SEBS-based sensor adheres directly to this surface, enabling simple peel-off replacement while preserving electrical contact (Video S3)[54]. A custom smartphone application enables real-time visualization, storage, and analysis of the eChem signal (Video S4).

Artifact-Corrected Personalized Glucose Monitoring

We first evaluated the cGEM on the body to determine whether its eChem output could be reliably converted to glucose concentration under conditions representative of routine earbud use. During wear, a meal was consumed to induce a physiological glucose excursion, while controlled changes in contact pressure, motion, and audio operation were introduced to assess interface-related artifacts (Fig. 4c). The WE1 and WE2 signals were acquired sequentially throughout the experiment. The WE1 response (with GOx) was benchmarked against a commercial CGM worn continuously, which provided the glucose profile used for comparison and calibration. WE1 exhibited a slowly varying glucose-dependent current that increased after meal consumption and subsequently declined in accordance with the CGM profile (Fig. 4c(i) to (iii)), demonstrating in-ear glucose sensing for the first time. Superimposed on this underlying trend were pronounced, rapid signal fluctuations associated with changes in applied pressure and motion (Fig. 4c(ii) and Fig. S18). In contrast, the enzyme-free WE2 channel showed minimal drift in its slowly varying baseline, but closely reproduced these rapid fluctuations, indicating that common-mode interferences were captured by both channels. As WE1 and WE2 differed in both signal amplitude and temporal behavior, adaptive mapping was used for artifact cancellation (Fig. S19). Accordingly, we implemented a dual-channel adaptive noise-cancellation framework based on an affine projection algorithm (APA) to selectively remove shared interference while preserving the underlying glucose-dependent response of WE1 (Figure 4c(iii)). A simplified schematic of the APA framework is shown in Fig. 4d, while further details are provided in Methods. The artifact-corrected WE1 signal was subsequently converted to glucose concentration using personalized calibration and subject-specific lag compensation, consistent with calibration strategies widely employed in previous CGM systems[49]. The resulting hybrid processing framework combined artifact cancellation, temporal alignment, and individualized current-to-glucose conversion. Before the APA-based artifact correction, the cGEM showed moderate agreement with the commercial CGM (Pearson r = 0.62), largely limited by the deliberately introduced mechanical disturbances (Fig. 4e). Following the APA processing, the correlation increased substantially to r = 0.90, demonstrating reliable recovery of glucose dynamics despite the non-fixed sensing interface.

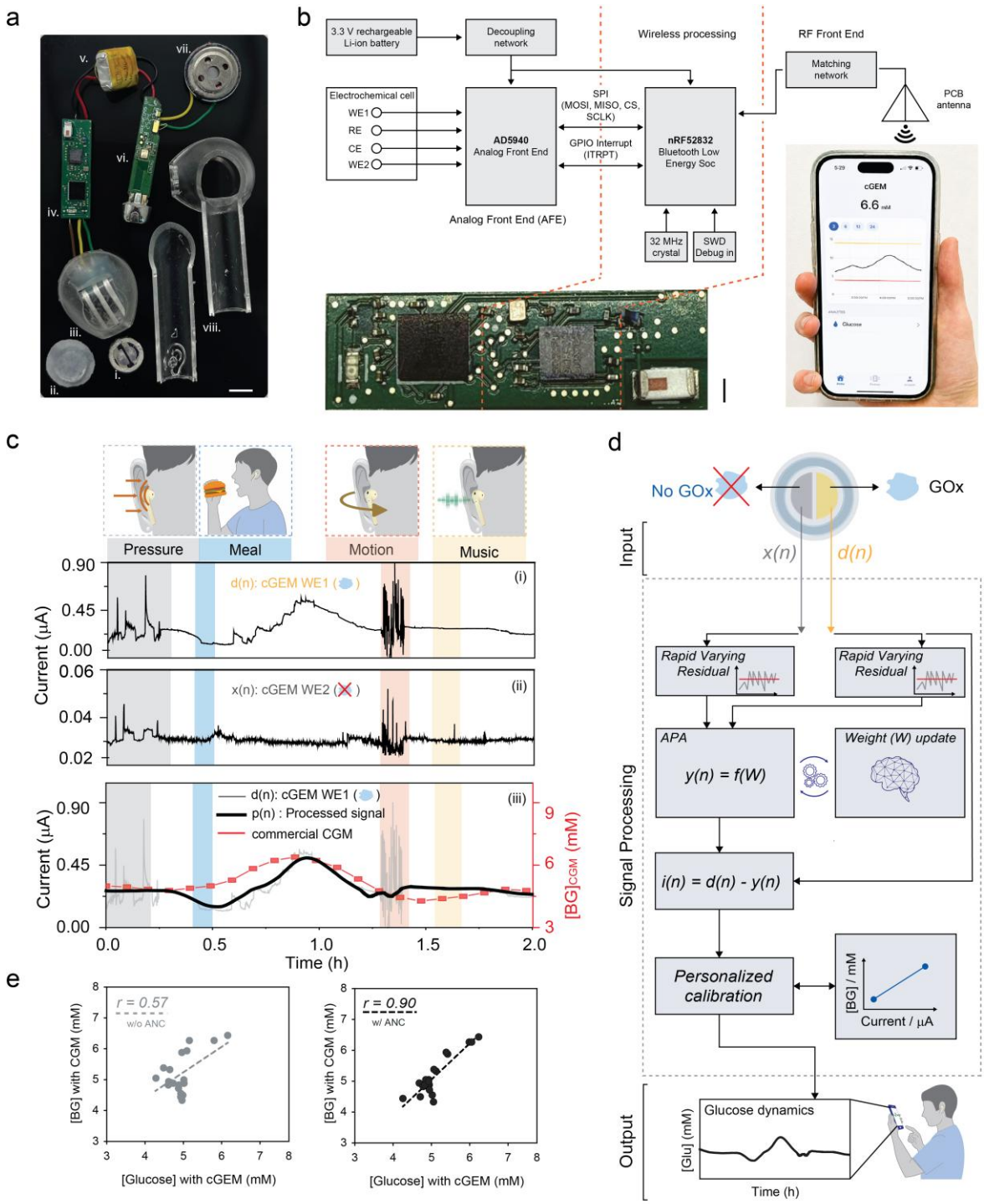


Figure 4: System integration and signal processing. a) *Exploded view of the integrated cGEM earbud showing the disposable glucose biosensor (i), fluidic module (ii), electrical interconnect interface (iii), sensing PCB (iv), rechargeable battery (v), audio PCB and charging interface (vi), speaker (vii), and earbud housing (viii). Scale bar, 7 mm.* ***b)*** *Sensing-electronics architecture. WE1 and WE2 are sequentially multiplexed to the AFE and share a*

common CE/RE. A photograph of the custom-designed sensing PCB is shown in the bottom panel. Scale bar, 2 mm. ***c)*** *Representative on-body signals during a meal-induced glucose excursion and controlled pressure, motion, and audio-related perturbations. i, Raw WE1 current, d(n). ii, sequentially acquired WE2 reference current, x(n). iii, APA-corrected WE1 signal, i(n), overlaid with raw d(n); corresponding commercial CGM blood glucose ([BG]) profile is shown in red.* ***d)*** *Hybrid signal-processing framework combining APA-based artifact correction and personalized calibration. d(n) served as the sensing channel (signal + noise), while the enzyme-free x(n) served as the reference channel (noise only). Rapidly varying x(n) is adaptively mapped to the correlated interference in d(n) using a function with an adaptively updated weight vector, f(W). The estimated artifact, y(n), is subtracted to obtain the corrected current, i(n), followed by personalized calibration and conversion to glucose concentration [Glu].* ***e)*** *Correlation of cGEM with blood glucose [BG] from commercial CGM before and after APA correction.*

Single-session on-body performance of cGEM

The cGEM was evaluated in four healthy individuals during continuous 5-h monitoring sessions, each including at least one glucose excursion induced by a high-sugar meal, snack, or beverage (Fig. 5a). The 5-h duration was selected to represent an extended yet practically relevant period of routine earbud use[55], while providing sufficient time to capture meal-induced glucose dynamics and subsequent recovery[23]. Whereas the cGEM was worn only during the defined sensing periods, the participants also wore a commercial CGM continuously on the arm for 10 days. The commercial CGM provided a continuous glucose reference profile (at 5-min intervals) for comparison (Fig. 5b). For each individual, the first glucose excursion was used to establish the personalized calibration parameters. Following each session, the raw cGEM WE1 and WE2 signals were processed using the hybrid artifact-correction and personalized-calibration framework to generate the final glucose concentration output. Across all four participants, cGEM closely followed major temporal glucose profiles measured by the commercial CGM, including the rise following glucose intake and the subsequent decline (Fig. 5b). The cGEM consistently captured glucose dynamics across participants despite inter-individual differences in ear anatomy, sensor contact, sweat characteristics, and physiological glucose responses. The ability to resolve distinct temporal glucose profiles further supports sustained operation of both the fluidic and sensing interfaces over the 5-h monitoring period. Tracking the rise and subsequent decline of each glucose excursion requires continuous replenishment of sweat at the sensing region, enabling the measured concentration to reflect newly secreted sweat rather than residual fluid retained within the patch. In the absence of such replenishment, mixing with previously collected sweat would attenuate transient concentration changes and delay signal recovery between successive events, consistent with the in vitro observations in Fig.

3e. These observations therefore provide functional evidence of continuous sweat replacement and sustained analyte transport through the paper-based fluidic patch. Quantitatively, the cGEM showed strong agreement with the commercial CGM across participants, with Pearson correlation coefficients (r) ranging from 0.81 to 0.88 (Fig. 5c). Mean absolute relative difference (MARD) remained at or below 15% across the measured glucose range of 60-130 mg dL^{-1}(Fig. 5d). Within this range, no significant dependence of MARD on glucose concentration or monitoring duration was observed (Fig. 5d), supporting applicability to the healthy cohort and stable performance over the entire 5-h sensing period. Across the measured glucose range, all paired cGEM–CGM measurements fell within Clarke error-grid zones A and B, with the majority located in zone A (>98%, $n = 273$) (Fig. 5e).

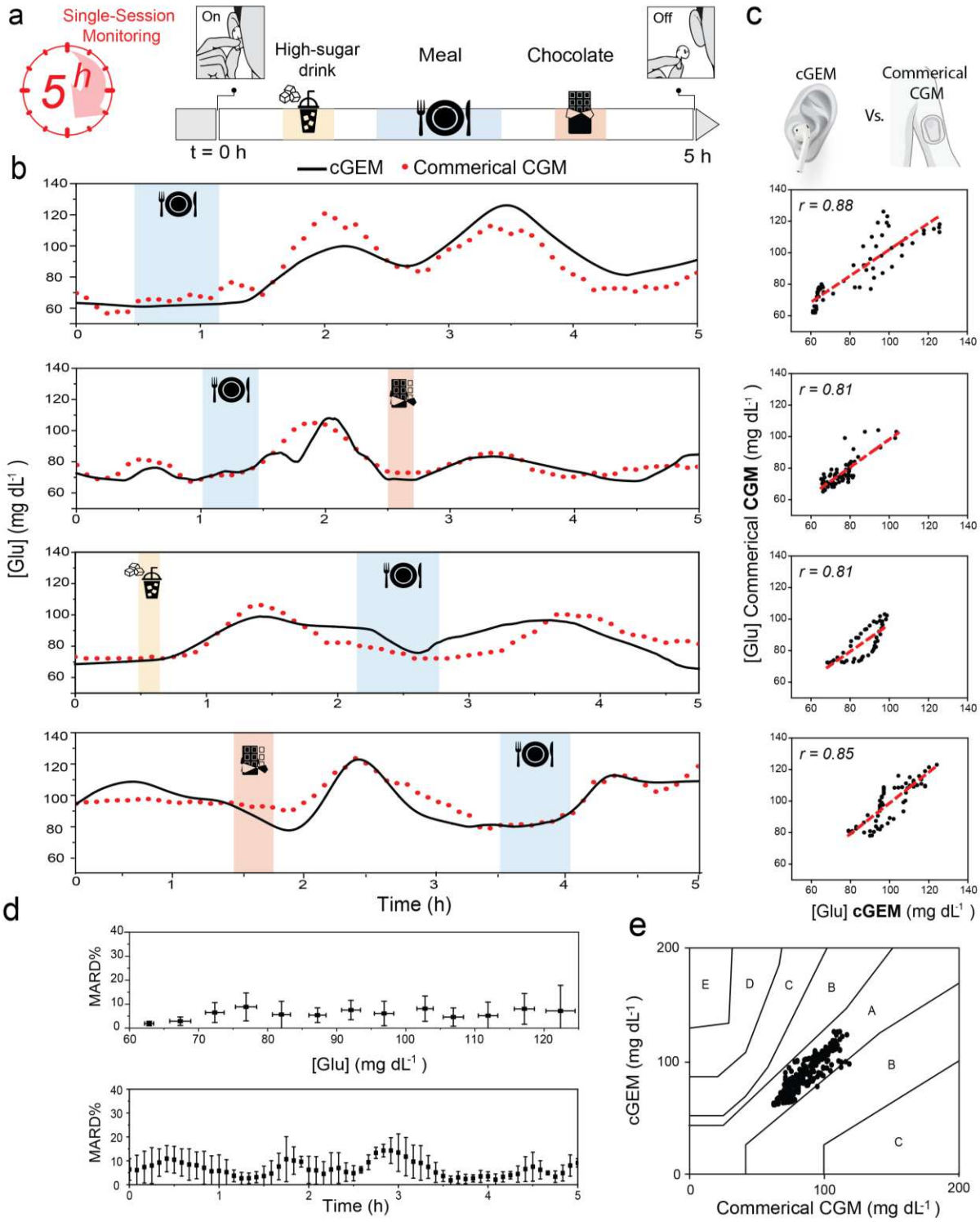


Figure 5: Single-session on-body performance of cGEM. a) *On-body study design comprising of 5-h cGEM monitoring in four healthy participants during meal-, snack- or beverage-induced glucose excursions, along with CGM monitoring using a commercial device.* ***b)*** *Temporal cGEM glucose profiles (black solid line) compared with the*

corresponding commercial CGM measurements (red dotted line) for the four participants. ***c)*** *Correlation between the cGEM and commercial CGM measurements, with Pearson correlation coefficients of r = 0.81 – 0.88.* ***d)*** *Mean absolute relative difference (MARD) as a function of glucose concentration and monitoring time.* ***e)*** *Clarke error-grid analysis of paired cGEM–CGM measurements (n = 273).*

Periodic on-body cGEM monitoring during daily activities

The cGEM was evaluated for periodic glucose monitoring during daily activities in all four participants (Fig. 6). This study was designed to determine whether periodic, on-demand cGEM measurements could accurately capture event-specific glucose responses while also reproducing the broader daily glucose dynamics. The cGEM sensing sessions were conducted at different times throughout the day, between 10 am and 7 pm, under representative real-world conditions, including consumption of high- and low-sugar beverages, different meals, snacks, exercise, and sedentary desk work (Fig. 6a). These activities were selected to encompass conditions expected to modulate physiological glucose levels while also representing common situations in which earbuds are routinely worn. The timing of each meal or activity varied relative to when the cGEM was first worn, with some events occurring before sensor placement and others during the sensing period, thereby reflecting the variable timing expected during real-world earbud use. For each sensing session, a new disposable sensing module was connected to the reusable earbud platform. The complete cGEM system was worn in the participant's ear for periods ranging approximately from 1.5 to 5 h, excluding an initial stabilization period of approximately 20 min. Across all four participants, diverse daily activities, and 13 sensing sessions, the cGEM closely reproduced the temporal glucose trends recorded by the continuously worn commercial CGM (Fig. 6b). The cGEM captured a wide range of glucose dynamics, including short- and long-duration excursions, responses of varying magnitude, and periods in which glucose levels remained relatively stable. Comparison of cGEM glucose measurements with the corresponding commercial CGM values across all periodic measurements showed close agreement, yielding a Pearson correlation coefficient of r = 0.88. This high level of performance was maintained despite the repeated insertion and removal of the cGEM, differences in participants, activity type, and the timing of cGEM wear relative to each event (Fig. 6c). Notably, the unprocessed eChem signals exhibited substantially greater fluctuations before ANC processing (Fig. S20-21), highlighting the role of ANC in suppressing nonspecific noise. These results demonstrate that the cGEM can be worn around an event of interest to characterize the associated glucose response (Fig. 6d). Across participants, we found that higher carbohydrate intakes were generally associated with larger postprandial glucose excursions, although the magnitude of the response varied between individuals.

Chocolate consumption also produced a pronounced glucose increase despite a lower total carbohydrate content, likely reflecting its relatively high proportion of rapidly available sugars. Conversely, intensive cycling and prolonged sedentary desk work were associated with decreases in glucose relative to the preceding baseline in several sessions. Next, we examined whether measurements collected periodically across multiple events could provide a representative estimate of the broader daily glucose profile. For each participant, glucose concentrations obtained during the cGEM sensing periods were combined to define the glucose range over the day (Fig. 6e). Across all individuals and events, glucose concentrations remained within the physiological range of 70–140 mg dl^{-1}. Mean glucose levels nevertheless differed between individuals, with participant 1 exhibiting values closer to 100 mg dL^{-1}, whereas the remaining participants generally exhibited lower values closer to 90 mg dL^{-1} (Table S4). By strategically selecting physiologically relevant events for monitoring, periodic cGEM measurements reproduced the daily glucose range recorded by the continuously worn commercial CGM with an accuracy of 88%, despite requiring only ~6 h of wear over 24 h (Fig. S22). How well the periodic monitoring represented the daily glucose range depended on the timing of cGEM use, particularly including periods of substantial glucose change, such as carbohydrate-rich meals or intensive physical activity. Excluding these sensing periods progressively reduced agreement with the daily glucose range measured by the commercial CGM (Fig. S22). These findings demonstrate that periodic cGEM monitoring can capture event-specific glucose responses and provide a representative daily glucose range in healthy individuals when timely used, and under the assumption of limited nighttime fluctuations.

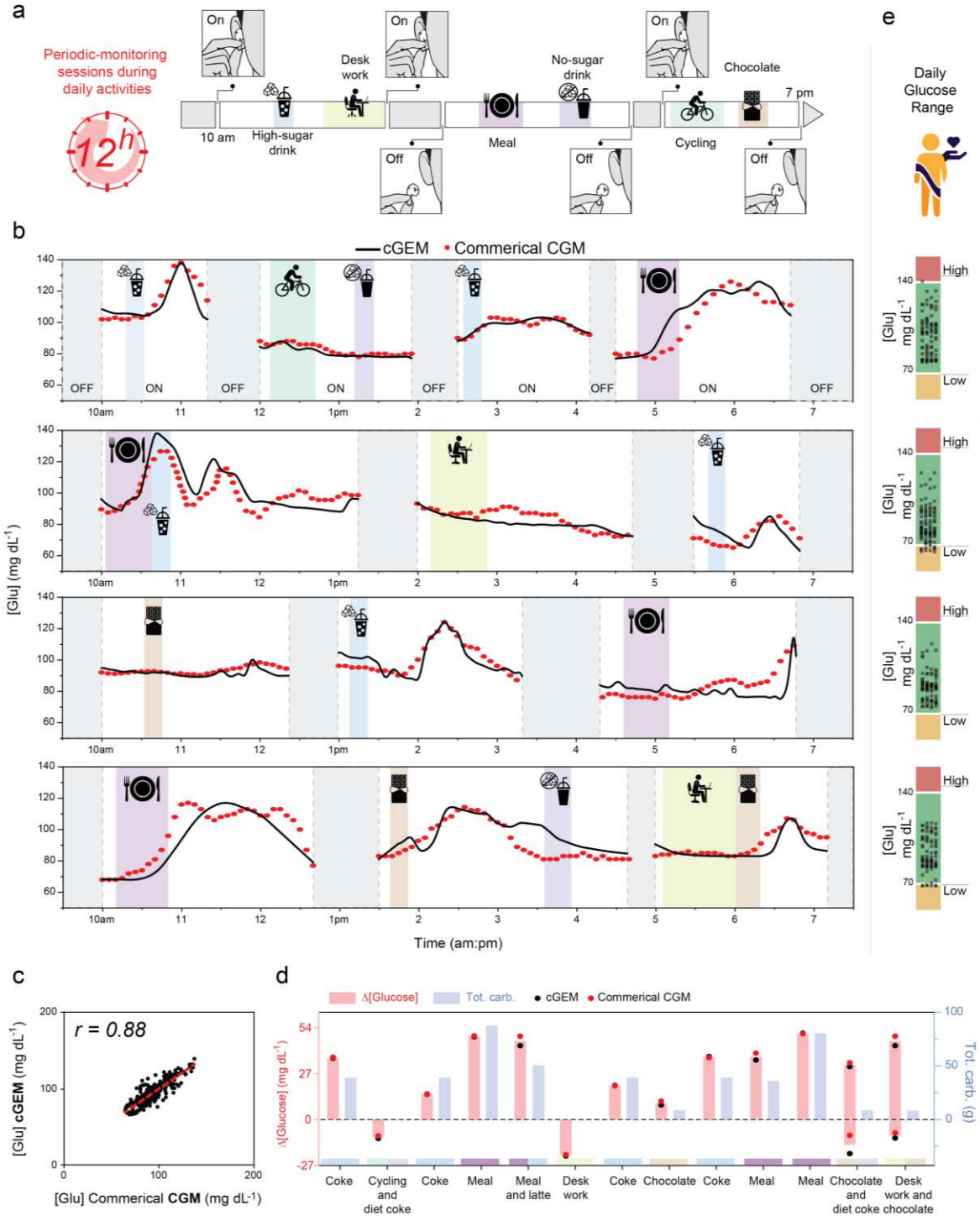


Figure 6: Periodic cGEM monitoring during daily activities. a) *On-body study design comprising of periodic cGEM sensing sessions conducted between 10 am and 7 pm. Each*

session lasted 1.5–4 h and included different dietary or activity-related events. ***b)*** *Temporal cGEM glucose profiles compared with the corresponding continuously worn commercial CGM measurements across four participants.* ***c)*** *Correlation between cGEM and the corresponding commercial CGM measurements across all periodic sensing sessions (n = 365 measurements), yielding a Pearson correlation coefficient of r = 0.88.* ***d)*** *Event-specific changes in glucose levels as a function of estimated carbohydrate intake across dietary or activity-related events.* ***e)*** *Estimation of the daily glucose range for each participant based on periodic cGEM measurements.*

Discussion

While continuous glucose monitoring has opened new opportunities for understanding glucose dynamics in wellness settings, conventional systems remain centered on prolonged, fixed wear. The cGEM explores a different mode of glucose monitoring in which sensing is embedded within a familiar earbud platform and used periodically around selected meals, activities, and other physiologically informative periods. This approach shifts the emphasis from prolonged wear of a dedicated wearable device toward a more flexible, seamlessly integrated platform that enables periodic access to the glucose dynamics during everyday life. Realizing this concept required addressing key challenges associated with in-ear sweat sensing, including sweat extraction, fluid handling, motion-related artifacts, and system-level integration. To meet these requirements, the cGEM combines a replaceable sensing module with a reusable earbud platform.

The sensing module was designed to maintain reliable sweat access and transport while supporting selective glucose detection in the confined in-ear environment. Osmotic sweat extraction coupled with evaporation-driven transport sustained stable fluid flow for more than 10 h. The GOx-based eChem biosensor provided a linear response across the physiologically relevant sweat glucose range with a limit of detection of 7 μM. An enzyme-free reference electrode was incorporated to capture non-specific fluctuations shared with the glucose-sensing channel for adaptive noise cancellation. This artifact correction improved the Pearson correlation between the cGEM and the continuously worn commercial arm-mounted CGM from 0.62 to 0.90, highlighting its importance for reliable sensing at a non-fixed wearable interface. The reusable earbud platform further enables the sensing module to be replaced without discarding the electronics. Miniaturized sensing and audio electronics are housed within the same earbud form factor and powered by a shared rechargeable battery for up to 5 h of operation. To relate the sweat-derived eChem signal to blood glucose concentration, a personalized calibration algorithm was applied using glucose excursions measured by a commercial CGM as reference. Across both extended and repeated daily monitoring sessions, the cGEM tracked glucose dynamics associated

with meals, beverages, exercise, and sedentary activity. Importantly, the device was repeatedly inserted and removed and was worn at different times relative to each event, reflecting how an earbud-based platform would be used in everyday life. The periodic monitoring results further demonstrated that the cGEM could capture glucose responses to specific events, while the timing of device use influenced how well these measurements represented broader daily glucose dynamics. Together, these findings establish in-ear sweat sensing as a potential route towards seamless glucose monitoring within an everyday wearable form factor. Rather than positioning cGEM as a replacement for a conventional CGM, the platform provides a complementary mode of access to glucose information that can be integrated into selected periods of daily life, either to examine the response to a specific physiological event or to obtain a representative view of daily glucose behavior. The cGEM earbud form factor thus offers a pathway to bringing glucose monitoring to millions of users who have not adopted conventional CGMs but could benefit from access to metabolic information. Future studies should evaluate cGEM across more diverse populations, including individuals with diabetes, where larger and more rapid glucose fluctuations are expected. Further work should assess long-term calibration stability and expand the platform toward multimodal monitoring of additional biochemical and physiological signals.

Methods

Sensor fabrication

The SEBS substrate was fabricated by casting a solution of styrene–ethylene–butylene–styrene (SEBS) onto a flat surface, followed by solvent evaporation to form a flexible polymer film. Sensing electrodes were patterned on the SEBS substrate using sputter deposition and stencil printing. Cr/Pt working electrodes were deposited through a patterned shadow mask, followed by stencil printing of the Ag/AgCl reference/counter electrode. Electrical connections were established by direct wiring or conductive vias. Both working electrodes underwent platinum electrodeposition. The enzymatic working electrode (WE1) was functionalized by sequential drop-casting of 4 µL of a 40 mg mL^{-1} GOx solution and 4 µL of 2% GA, while the second working electrode (WE2) was left untreated. Additional fabrication details, including the chemicals and materials list, are provided in Supplementary Information Note #1.

cGEM assembly

A customized potentiostat board and a commercial audio module were electrically connected in parallel to a rechargeable lithium-ion battery (Figure 4a). The audio module remained fully functional, retaining its original speaker and charging circuitry. The potentiostat was connected through extension wires to Ag/AgCl electrode traces patterned

on a SEBS substrate attached to the earbud cap, where the biosensor was positioned. All components were subsequently integrated within the 3D-printed earbud casing, which was sealed to secure the components and protect the internal electronics. Further details on the electronic design and integration are provided in Supporting Information Note #1 and #2.

In vitro testing

All in vitro experiments were performed under ambient laboratory conditions unless otherwise stated. eChem characterization was conducted using CA and CV under the specified experimental conditions in Supporting Note #3. Flow experiments were performed using a syringe pump to simulate sweat secretion. The limit of detection was determined using the 3σ/slope criterion, and sensor performance was evaluated against reference glucose measurements obtained using a commercial glucometer.

Numerical modeling

A transient finite-element model was used to solve the coupled Navier–Stokes and Nernst–Planck equations for fluid and mass transport within the system. The model assumed mass conservation and incompressible creeping flow. Fluid properties were approximated as water, with a glucose diffusion coefficient equals to 6.7×10^{-10} m^2 s^{-1}. Evaporation from the exposed paper surfaces was implemented as an outward fluid-flux boundary condition, with the evaporation rate estimated using a previously reported model[50]. To simulate discrete sweat secretion events, the analyte influx at the hydrogel surface was prescribed as a time-dependent rectangular function. Additional details are provided in Supplementary Note #4.

Adaptive noise cancellation

WE1 and WE2 currents (denoted d(n)and x(n), respectively, where n is the sample index) were processed using a dual-channel adaptive noise-cancellation (ANC) framework (Figure 4d). d(n) served as the sensing channel (signal + noise), while the enzyme-free x(n) served as the reference channel (noise only). A centered moving-average window of 100 samples separated each channel signal into a slowly varying trend and a rapidly varying residual. An affine projection algorithm (APA), with an 80-sample reference history and a projection order of 2, adaptively updated the filter-weight vector (***W***) to map the rapidly varying x(n) residual onto the corresponding d(n) residual. The resulting interference estimate, y(n), was subtracted from the original d(n) current to obtain the processed signal, i(n) = d(n) - y(n). Further details of trend separation, adaptive filtering and parameter selection are provided in Supplementary Note #5.

Personalized calibration

The cGEM signal, i(t), was calibrated against glucose concentrations measured by a commercial CGM using a personalized calibration model (Eqn.1), consistent with calibration approaches employed in other CGM systems[49]. For each individual, calibration was established from the maximum blood-glucose change, ΔBG, to the corresponding current change, Δi_{MAX}. A normalization term, $i(0)/i_0$, was used to account for differences in the initial cGEM current between sensing sessions, including baseline offsets associated with sensor-to-sensor, placement and interface variations.

$$C(t) = \frac{\Delta BG}{\Delta i_{MAX}}\left(i(t)\frac{i(0)}{i_0} - i_{MAX}\right) + BG_{MAX} \quad \text{(Eqn. 1)}$$

where $i(t)$ and $i(0)$ are the artifact-corrected cGEM currents at time t and at the start of the sensing session, respectively. The calibration parameters i_0, ΔBG, Δi_{MAX}, and BG_{MAX} represent the initial cGEM current, maximum blood-glucose change, corresponding cGEM current change, and maximum blood-glucose concentration, respectively. These were determined once from the glucose-excursion calibration session and were subsequently applied to all measurements from the same individual. A subject-specific temporal offset was additionally applied to account for the physiological lag between the blood and sweat glucose dynamics and fluid transport through the cGEM sampling system. Further details can be found in Supporting Note #5.

On body testing

Participants included female and male adults across a range of ages (20-35) and nationalities to capture broader demographic variability. Participants wore a commercial CGM (Lingo, Abbott) for at least 2 h before testing and continuously thereafter. Before cGEM insertion, the ear was cleaned and dried, and the hydrogel–paper fluidic components were assembled onto the earbud. The first ~20 min were excluded to account for sensor-dependent stabilization. Participants then performed predefined activities according to the study protocol. After testing, the hydrogel remained attached to the paper, with no residual material observed in the ear. All on-body experiments followed IRB00002758. Further details can be found in Supporting Note #6.

Author contributions

B.S. and J.W. conceived the idea. B.S., C.G., and E.V.S. contributed equally. B.S., C.G., E.V.S., M.M., L.C., M.I.K., Q.Y., K.G., V.P., T.S., M.P., Y.L., and M.R. performed experiments. B.S. and P.B. performed numerical simulations. B.S., C.G., E.V.S., L.C., M.I.K., K.G., M.P., Y.L., and M.R. fabricated, tested, and characterized the electrochemical sensors. M.M., G.J., and O.D. developed the electronics. B.S., E.V.S., and V.P. designed the CAD models and fabricated the

mechanical components of the device. B.S. and J.W. designed human studies. B.S., C.G., E.V.S., L.C, Q.Y., and J.W. analyzed the data. B.S., C.G., E.V.S., M.M., Q.Y., V.P., F.A., and J.W. contributed to writing, reviewing, and editing. J.W. supervised the project. All authors substantially contributed to the research and reviewed the manuscript.

Acknowledgements

This research was supported by the UCSD Center of Wearable Sensors (CWS). The authors would like to thank UCSD's Nano3 cleanroom. B.S. acknowledges support from Fulbright Israel. E.V.S. acknowledges support from Fulbright Switzerland.

Data availability

All data supporting the findings of this study are available within the article and its supplementary files. Any additional requests for information can be directed to, and will be fulfilled by, the corresponding authors.

Funding

No applicable funding.

Competing interests

The authors declare no competing interests.

Additional information

- **Supporting main file:** Additional experimental details, figures, tables, and supporting analyses.
- **Supporting Video S1:** Demonstration of Sensor Durability
- **Supporting Video S2:** Showcase of Earbud Charging Case
- **Supporting Video S3:** Concept demonstration of simple sensor placement and electrical connection
- **Supporting Video S4:** Real-Time Data Collection Through a Mobile App

Correspondence and requests for materials should be addressed to Joseph Wang.

References

1. Kim, J., Campbell, A. S., De Ávila, B. E.-F. & Wang, J. Wearable biosensors for healthcare monitoring. *Nat. Biotechnol.* **37**, 389–406 (2019).

2. Battelino, T. *et al.* Clinical Targets for Continuous Glucose Monitoring Data Interpretation: Recommendations From the International Consensus on Time in Range. *Diabetes Care* **42**, 1593–1603 (2019).

3. Ajjan, R. A. *et al.* Continuous glucose monitoring for the routine care of type 2 diabetes mellitus. *Nat. Rev. Endocrinol.* **20**, 426–440 (2024).

4. Garg, S. K. *et al.* Accuracy and Safety of Dexcom G7 Continuous Glucose Monitoring in Adults with Diabetes. *Diabetes Technol. Ther.* **24**, 373–380 (2022).

5. Teymourian, H., Barfidokht, A. & Wang, J. Electrochemical glucose sensors in diabetes management: an updated review (2010–2020). *Chem. Soc. Rev.* **49**, 7671–7709 (2020).

6. Jarvis, P. R. E., Cardin, J. L., Nisevich-Bede, P. M. & McCarter, J. P. Continuous glucose monitoring in a healthy population: understanding the post-prandial glycemic response in individuals without diabetes mellitus. *Metabolism* **146**, 155640 (2023).

7. Bermingham, K. M. *et al.* Associations of continuous glucose monitor derived time in range and glycaemic variability with diet lifestyle and demographics. *Nat. Commun.* **17**, 4496 (2026).

8. Klonoff, D. C. *et al.* Use of Continuous Glucose Monitors by People Without Diabetes: An Idea Whose Time Has Come? *J. Diabetes Sci. Technol.* **17**, 1686–1697 (2023).

9. Rigo, R. S. *et al.* Cutaneous Reactions to Continuous Glucose Monitoring and Continuous Subcutaneous Insulin Infusion Devices in Type 1 Diabetes Mellitus. *J. Diabetes Sci. Technol.* **15**, 786–791 (2021).

10. Seibold, A. Minimizing Adverse Skin Reactions to Wearable Continuous Glucose Monitoring Sensors in Patients With Diabetes. *J. Diabetes Sci. Technol.* **15**, 713–714 (2021).

11. Genève, P. *et al.* High incidence of skin reactions secondary to the use of adhesives in glucose sensors or insulin pumps for the treatment of children with type 1 diabetes. *Diabetes Res. Clin. Pract.* **204**, 110922 (2023).

12. Rodbard, D. Continuous Glucose Monitoring: A Review of Successes, Challenges, and Opportunities. *Diabetes Technol. Ther.* **18**, (2016).

13. Poolsup, N., Suksomboon, N. & Kyaw, A. M. Systematic review and meta-analysis of the effectiveness of continuous glucose monitoring (CGM) on glucose control in diabetes. *Diabetol. Metab. Syndr.* **5**, 39 (2013).

14. Edelman, S. V., Argento, N. B., Pettus, J. & Hirsch, I. B. Clinical Implications of Real-time and Intermittently Scanned Continuous Glucose Monitoring. *Diabetes Care* **41**, 2265–2274 (2018).

15. Mansour, M., Saeed Darweesh, M. & Soltan, A. Wearable devices for glucose monitoring: A review of state-of-the-art technologies and emerging trends. *Alex. Eng. J.* **89**, 224–243 (2024).

16. Flynn, C. D. *et al.* Biomolecular sensors for advanced physiological monitoring. *Nat. Rev. Bioeng.* **1**, 560–575 (2023).

17. Saha, T. *et al.* Wearable Electrochemical Glucose Sensors in Diabetes Management: A Comprehensive Review. *Chem. Rev.* **123**, 7854–7889 (2023).

18. Kim, J., Campbell, A. S. & Wang, J. Wearable non-invasive epidermal glucose sensors: A review. *Talanta* **177**, 163–170 (2018).

19. Brasier, N. & Eckstein, J. Sweat as a Source of Next-Generation Digital Biomarkers. *Digit. Biomark.* **3**, 155–165 (2019).

20. Wang, J. Electrochemical Glucose Biosensors. *Chem. Rev.* **108**, 814–825 (2008).

21. Wang, M. *et al.* A wearable electrochemical biosensor for the monitoring of metabolites and nutrients. *Nat. Biomed. Eng.* **6**, 1225–1235 (2022).

22. Moyer, J., Wilson, D., Finkelshtein, I., Wong, B. & Potts, R. Correlation Between Sweat Glucose and Blood Glucose in Subjects with Diabetes. *Diabetes Technol. Ther.* **14**, 398–402 (2012).

23. Saha, T. *et al.* A Passive Perspiration Inspired Wearable Platform for Continuous Glucose Monitoring. *Adv. Sci.* **11**, 2405518 (2024).

24. Bandodkar, A. J., Jia, W. & Wang, J. Tattoo-Based Wearable Electrochemical Devices: A Review. *Electroanalysis* **27**, 562–572 (2015).

25. Bandodkar, A. J. *et al.* Tattoo-Based Noninvasive Glucose Monitoring: A Proof-of-Concept Study. *Anal. Chem.* **87**, 394–398 (2015).

26. Martín, A. *et al.* Epidermal Microfluidic Electrochemical Detection System: Enhanced Sweat Sampling and Metabolite Detection. *ACS Sens.* **2**, 1860–1868 (2017).

27. Cho, S. *et al.* A skin-interfaced microfluidic platform supports dynamic sweat biochemical analysis during human exercise. *Sci. Transl. Med.* **16**, eado5366 (2024).

28. Mei, X. *et al.* Wearable three-dimensional paper-based microfluidic electrochemical sensors for real-time sweat monitoring. *Chem. Eng. J.* **515**, 163786 (2025).

29. Li, M. *et al.* A highly integrated sensing paper for wearable electrochemical sweat analysis. *Biosens. Bioelectron.* **174**, 112828 (2021).

30. Ding, S. *et al.* A fingertip-wearable microgrid system for autonomous energy management and metabolic monitoring. *Nat. Electron.* **7**, 788–799 (2024).

31. Bae, C. W. *et al.* Fully Stretchable Capillary Microfluidics-Integrated Nanoporous Gold Electrochemical Sensor for Wearable Continuous Glucose Monitoring. *ACS Appl. Mater. Interfaces* **11**, 14567–14575 (2019).

32. Cai, S. *et al.* Air-permeable electrode for highly sensitive and noninvasive glucose monitoring enabled by graphene fiber fabrics. *Nano Energy* **93**, 106904 (2022).

33. Djassemi, O. *et al.* A Touch Enabled Hemodynamic and Metabolic Monitor. *Adv. Sci.* **12**, 2502138 (2025).

34. Yin, L. *et al.* A stretchable epidermal sweat sensing platform with an integrated printed battery and electrochromic display. *Nat. Electron.* **5**, 694–705 (2022).

35. Zhao, J. *et al.* A Fully Integrated and Self-Powered Smartwatch for Continuous Sweat Glucose Monitoring. *ACS Sens.* **4**, 1925–1933 (2019).

36. Yu, Y., Nyein, H. Y. Y., Gao, W. & Javey, A. Flexible Electrochemical Bioelectronics: The Rise of In Situ Bioanalysis. *Adv. Mater.* **32**, 1902083 (2020).

37. Gong, S., Lu, Y., Yin, J., Levin, A. & Cheng, W. Materials-Driven Soft Wearable Bioelectronics for Connected Healthcare. *Chem. Rev.* **124**, 455–553 (2024).

38. Kim, C. Y. *et al.* Wireless Technologies for Wearable Electronics: A Review. *Adv. Electron. Mater.* **11**, 2400884 (2025).

39. Chen, S. *et al*. Wearable flexible microfluidic sensing technologies. *Nat. Rev. Bioeng.* **1**, 950–971 (2023).

40. Kim, J., Campbell, A. S., De Ávila, B. E.-F. & Wang, J. Wearable biosensors for healthcare monitoring. *Nat. Biotechnol.* **37**, 389–406 (2019).

41. Chan, J., Goel, M., Gollakota, S. & Nandakumar, R. Mobile medical systems for equitable healthcare. *Nat. Rev. Bioeng.* **3**, 855–874 (2025).

42. Röddiger, T. *et al.* Sensing with Earables: A Systematic Literature Review and Taxonomy of Phenomena. *Proc. ACM Interact. Mob. Wearable Ubiquitous Technol.* **6**, 1–57 (2022).

43. Martin, A. & Voix, J. In-Ear Audio Wearable: Measurement of Heart and Breathing Rates for Health and Safety Monitoring. *IEEE Trans. Biomed. Eng.* **65**, 1256–1263 (2018).

44. He, D. D., Winokur, E. S. & Sodini, C. G. An Ear-Worn Vital Signs Monitor. *IEEE Trans. Biomed. Eng.* **62**, 2547–2552 (2015).

45. Zhang, W. *et al.* Continuous Core Body Temperature Monitoring for Heatstroke Alert via a Wearable In-Ear Thermometer. *ACS Sens.* **10**, 1440–1449 (2025).

46. Clarke, L., Liau, C., Wei, V. W. & Liao, C. Healthcare monitoring with earables: A paradigm shift towards digital health. *Biomed. Anal.* **2**, 207–222 (2025).

47. Xu, Y. *et al.* In-ear integrated sensor array for the continuous monitoring of brain activity and of lactate in sweat. *Nat. Biomed. Eng.* **7**, 1307–1320 (2023).

48. Kaongoen, N. *et al.* The future of wearable EEG: a review of ear-EEG technology and its applications. *J. Neural Eng.* **20**, 051002 (2023).

49. Saha, T. *et al.* A fully integrated smart ring for daily biochemical monitoring. *Nat. Commun.* **17**, 9003 (2026).

50. Shay, T., Saha, T., Dickey, M. D. & Velev, O. D. Principles of long-term fluids handling in paper-based wearables with capillary–evaporative transport. *Biomicrofluidics* **14**, 034112 (2020).

51. Cao, Q. *et al.* Three-dimensional paper-based microfluidic electrochemical integrated devices (3D-PMED) for wearable electrochemical glucose detection. *RSC Adv.* **9**, 5674–5681 (2019).

52. Wang, J. Electrochemical Glucose Biosensors. *Chem. Rev.* **108**, 814–825 (2008).

53. House, J. L., Anderson, E. M. & Ward, W. K. Immobilization Techniques to Avoid Enzyme Loss from Oxidase-Based Biosensors: A One-Year Study. *J. Diabetes Sci. Technol.* **1**, 18–27 (2007).

54. Khan, M. I. *et al.* A smart cup for wireless, biofuel-powered, sweat-based vitamin C sensing. *Biosens. Bioelectron.* **292**, 118100 (2026).

55. Shah, P., Dave, P., Das, L., Shah, U. & Bharadva, N. Patterns and perceived risks of personal auditory device use among medical students: a cross-sectional study. *BMC Res. Notes* **18**, 462 (2025).

Supplementary Files

This is a list of supplementary files associated with this preprint. Click to download.

- VideoS2Showcaseofearbudcase.mov
- VideoS3Conceptdemonstrationofsimplesensorplacementandelectricalconnection.mov
- SupplementaryInformation.docx
- VideoS4RealTimeDataCollectionThroughaMobileApp.mov
- VideoS1DemonstrationofSensorDurability.mov